Journal of ELECTRONIC MATERIALS, Vol. 40, No. 9, 2011
DOI: 10.1007/s11664-011-1702-1

Impact of Isothermal Aging on Long-Term Reliability of Fine-Pitch Ball Grid Array Packages with Sn-Ag-Cu Solder Interconnects: Die Size Effects

TAE-KYU LEE,[1,3] WEIDONG XIE,[1] BITE ZHOU,[2] THOMAS BIELER,[2] and KUO-CHUAN LIU[1]

1.—Component Quality and Technology Group, Cisco Systems, Inc., San Jose, CA 95134, USA. 2.—Michigan State University, East Lansing, MI, USA. 3.—e-mail: taeklee@cisco.com

The interaction between isothermal aging and long-term reliability of fine-pitch ball grid array (BGA) packages with two different die sizes was investigated. Both 5 mm × 5 mm and 10.05 mm × 10.05 mm die-attached packages with Sn-3.0Ag-0.5Cu (wt.%) solder balls were used to compare the correlation between the internal strain difference and isothermal aging on microstructural evolution during thermal cycling. To determine their long-term reliability, the samples were isothermally aged and thermally cycled from 0°C to 100°C with 10-min dwell time. Based on Weibull plots for each aging condition, the packages with large dies attached showed shorter characteristic lifetimes, because of the relatively higher stress, but showed less lifetime degradation with isothermal aging compared with the smaller die-attached samples. Microstructure analysis using orientation imaging microscopy (OIM) revealed the evolution of the microstructure during thermal cycling, showing a higher degree of recrystallization inside the bulk solder for joints that were isothermally aged and experienced higher stress. The possible mechanisms giving rise to these observations are discussed.

Key words: Pb-free solder, isothermal aging, microstructure, OSP surface finish, orientation image microscopy (OIM)

INTRODUCTION

The recent trend in electronics toward higher functionality in a given limited space has led the industry toward higher-density packages, which require an increased number of interconnections per component.[1,2] This technological trend presents several challenges, because as solder joints become smaller, they are expected to become more affected by the thickness and morphology of the solder joint interface intermetallic compounds (IMC) and more sensitive to the local chemical composition of the bulk solder alloy, which are affected by the microstructural evolution and surface finish of the packages and boards.[3–6] In addition to these factors, the overall increase in stress produced by the increasing mismatch between the coefficients of thermal expansion (CTE) reduces the overall thermal fatigue lifetime of the package.

In recent publications, it has been shown that thermal aging effects are more severe for Sn-based Pb-free solders than for eutectic Sn-Pb solder alloys, posing potentially higher risks for implementation of Pb-free solders for longer operation life; moreover, it is known that the microstructure changes dramatically during thermal aging.[7–12] A recent study showed the isothermal aging impact on thermal fatigue performance, and a possible theory was explained.[13] It was observed that NiAu-surface-finished fine-pitch packages are greatly affected by isothermal aging, with a lifetime reduction of more than 40% relative to the characteristic lifetime. It was also reported that the organic surface pre-

(Received October 25, 2010; accepted June 8, 2011; published online June 29, 2011)

servative (OSP) surface finish has a relatively minor impact on this package configuration compared with NiAu-surface-finished samples. Both fine-pitch packages used in the study can be categorized as "high-stress" packages because they feature a large silicon die size (10.05 mm × 10.05 mm), which builds up a relatively higher stress at the solder joints due to a higher CTE mismatch.

In this study, the thermal cycling performance and, thus, the long-term reliability were observed with the variation of the internal stress due to the different silicon die sizes. Focusing on the package-side microstructure, the impact of isothermal aging on both the small- and large-die-attached samples was analyzed by using polarized filtered optical microscopy; the impact of recrystallization was also investigated. Along with optical microscopy observation, Sn grain orientation associated with the thermal cycling and isothermal aging effect was investigated using orientation image microscopy (OIM).

EXPERIMENTAL PROCEDURES

Figure 1 shows the samples used in this study, which were 13 mm × 13 mm body size ball grid arrays (BGAs) with a four-row perimeter array and a total of 432 solder joints. The solder ball diameter was 300 μm, and they were arranged in the package with a 0.4 mm pitch, which is the distance between the mid points of each solder. The composition of the solder balls used in this study was Sn-3.0Ag-0.5Cu (wt.%) (SAC305). Two die sizes were selected; one group of packages had 10.05 mm × 10.05 mm and the other group of samples had 5 mm × 5 mm silicon die attached. The package-side substrates had OSP surface finish on top of the Cu substrate. Parts were attached to a 2.4-mm-thick 370HR printed circuit board with glass-transition temperature (T_g) of over 170°C with OSP surface finish on top of Cu. Sn-3.0Ag-0.5Cu (wt.%) (SAC305) solder paste was used for the board assembly reflow with typical peak temperature of 240°C and 60 s above the liquidus temperature.

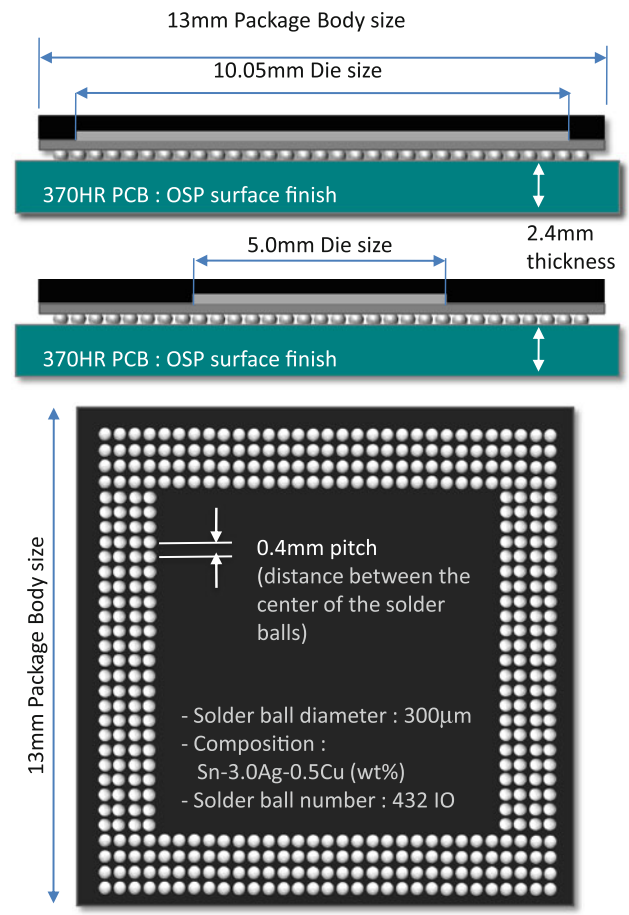

Fig. 1. Fine-pitch BGA sample configuration.

For pretreatment prior to thermal cycling, samples were isothermally aged at either 100°C or 150°C, with holding time ranging between 500 h and 1000 h, in ambient air. For thermal cycling, samples were tested with a 0°C to 100°C thermal cycle, a ramp rate of 10°C/min, and 10 min dwell time. All components were daisy-chained parts, and continuous resistivity measurement was applied for *in situ* monitoring during the test. The failure criterion in this study was a 20% increase of peak resistivity compared with the initial value. The thermal cycling results are plotted in Weibull distribution plots, and the statistical characteristic lifetime cycles for each thermal aging condition was identified from the plot. Failed samples were subjected to cross-section and dye-and-pry analysis to observe the evolution of the microstructure and the location of the failed solder joint. For Sn grain orientation analysis, selected joints were imaged using both polarized light microscopy and orientation imaging microscopy (OIM) as described in prior works.[14–17] Measured data were analyzed using OIM Analysis software (version 5.31) to generate orientation joint scan images.

RESULTS AND DISCUSSION

Figure 2 shows the initial microstructure right after board assembly and after isothermal aging. As shown in Fig. 2a, d, the OSP-surface-finished samples right after board assembly showed scallop-shaped IMCs at both the package-side (Fig. 2a) and the board-side interface (Fig. 2d). Fine, networked IMC precipitates are observed in the as-assembled sample compared with the coarsened and accumulated precipitates in the joints after isothermal aging, as shown in Fig. 2b, c and e, f. Relatively steady growth of the IMC precipitates, gradual change of the interface IMC morphology to a uniform thickness, and a thicker Cu_3Sn intermetallic layer were also observed with longer aging times and higher aging temperatures.

Figure 3 shows a Weibull plot for the thermal cycling results from large- and small-die-attached

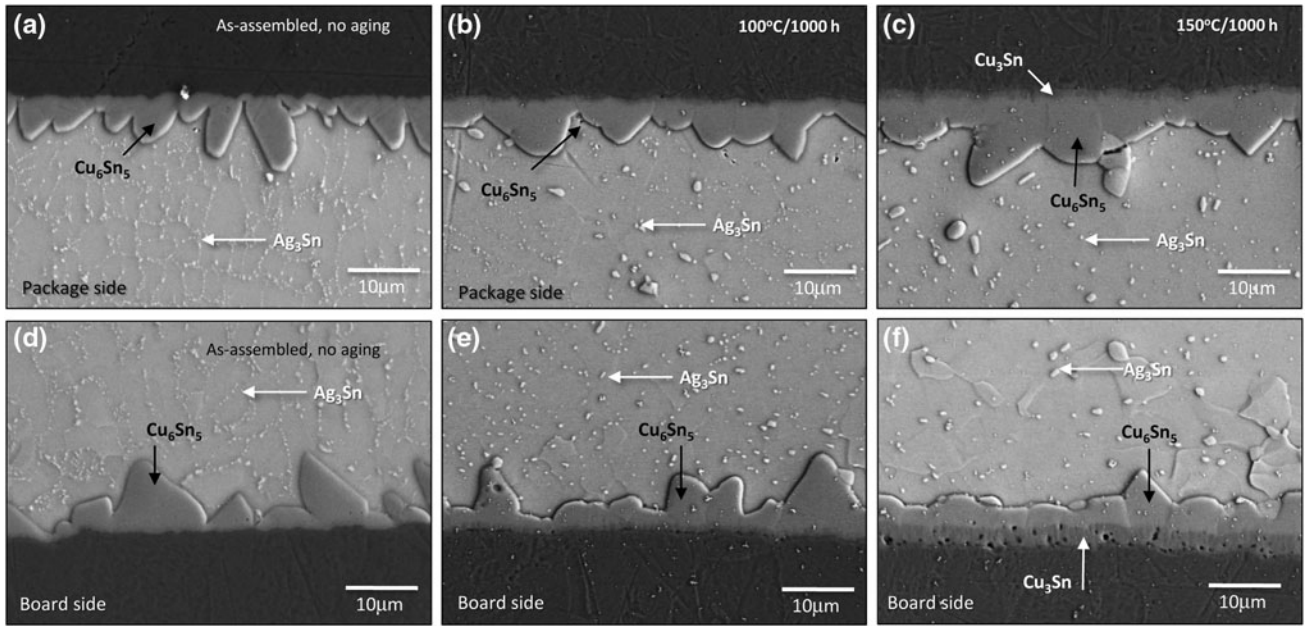

Fig. 2. SEM microstructure before and after isothermal aging: package-side interface (a) as-assembled, (b) after 100°C/1000 h aging, and (c) after 150°C/1000 h aging; board-side interface (d) as-assembled, (e) after 100°C/1000 h aging, and (f) after 150°C/1000 h aging.[13]

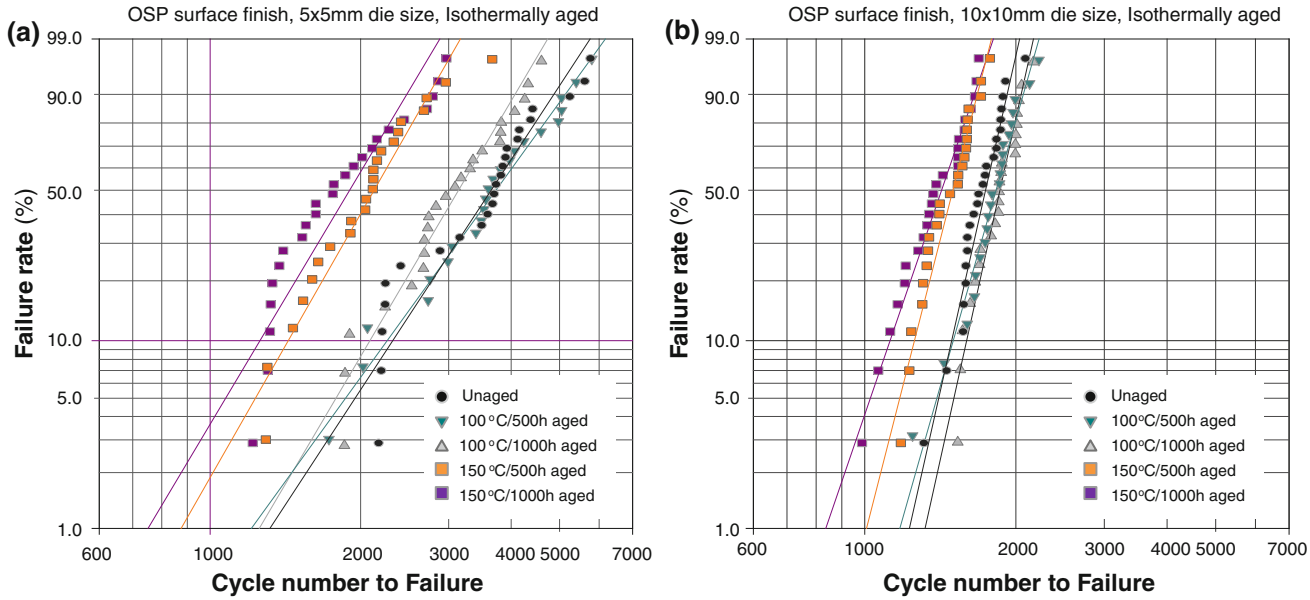

Fig. 3. Weibull plot for the thermal cycling results on the isothermally aged BGA samples: (a) small-die (5 mm× 5 mm) attached packages and (b) large-die (10 mm × 10 mm) attached package samples.

BGA samples with and without isothermal aging pretreatment. Twenty-four samples were tested for each precondition. Figure 3a shows the results for the small (5 mm × 5 mm) die-attached packages. The first failure occurred at around 2200 cycles for the unaged, as-assembled condition. Overall, the smaller die-attached sample set showed much longer thermal fatigue lifetime than the large (10.05 mm × 10.05 mm) die-attached samples, which showed the first failure at around 1200 cycles for the unaged, as-assembled condition. Considering the characteristic lifetime cycle number, which is the cycle number at a 63.5% failure rate, the characteristic life cycle number for unaged, as-assembled small die samples was 4112 cycles. The large die samples showed a characteristic life cycle number of 1915 cycles, an approximately 53% lower lifetime compared with that of the small-die as-assembled samples. Thermal cycling results after isothermal aging pretreatment showed a degradation of the characteristic lifetime cycle number for both small- and large-die-attached samples.

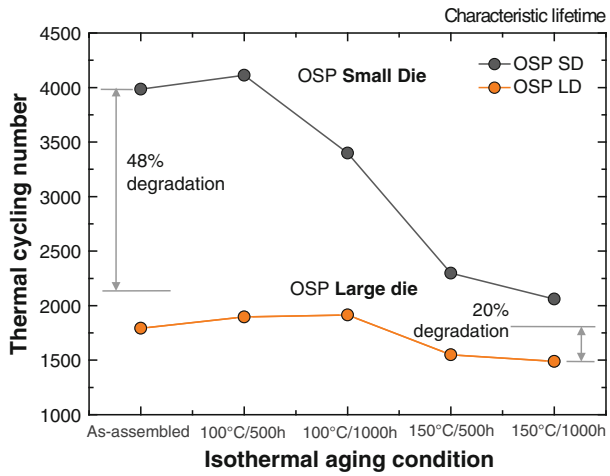

Fig. 4. Characteristic lifetime cycle number summary plot for small- and large-die-attached OSP samples for each precondition.

However, compared with the characteristic life of the larger die samples, the smaller die-attached samples showed a higher rate of degradation after isothermal aging. As shown in Fig. 3a, the characteristic lifetime after aging at 150°C for 1000 h was reduced to 2298 cycles. This represents a 49% reduction in lifetime, and even at 500 h of aging, the amount of degradation was similar to that of the 1000 h aging samples. Compared with these small-die-attached samples, the large-die-attached samples in Fig. 3b showed a relatively slower degradation rate, a result that was recently published in Ref. 13. The characteristic lifetime cycles for unaged samples and 150°C/1000 h aged samples were 1897 cycles and 1489 cycles, respectively, which is approximately a 20% reduction of lifetime.

Figure 4 shows a summary plot of the characteristic lifetime for each precondition for small- and large-die-attached samples. The small-die-attached samples showed higher characteristic life cycle numbers for the unaged condition but a gradual decrease with higher temperatures and longer aging times. Compared with the small die size data, the large die samples showed a much lower cycle number at the beginning but maintained the characteristic life cycle number even after aging at 150°C for 1000 h.

In Ref. 13, the comparison between electrolytic NiAu- and OSP-surface-finished samples revealed different effects of isothermal aging impact, which was higher for the electrolytic NiAu-surface-finished samples because of the precipitate depletion zone at the package-side bulk solder. The unbalanced chemical composition structure in NiAu-surface-finished samples was suggested as the main reason and driving force for the depletion zone. The reduced isothermal aging impact on OSP-surface-finished samples was explained by the balanced Cu-solder-Cu structure (Cu at both the package- and board-side interfaces), which mitigated depletion zone formation. However, the results presented herein actually show that, even if the joint has a balanced Cu-solder-Cu structure, the isothermal aging impact can affect the lifetime by up to 49%. The possible explanation for the isothermal aging impact in small-die-attached OSP-surface-finished packages can be found in the relatively long total thermal cycling time compared with that of the large-die-attached OSP-surface-finished packages; for example, the large-die-attached sample characteristic lifetime cycles to failure with 100°C/1000 h aging was 1915 cycles, which was approximately 47 days in the thermal cycling chamber. Compared with this, the small-die-attached samples with 100°C/1000 h aging failed at 3399 cycles, which was after 85 days. The overall characteristic lifetime cycle number was reduced from 4112 cycles to 2298 cycles for the small-die-attached samples before and after thermal aging at 150°C. Although this represents a 49% decrease, both characteristic lifetime cycle numbers are still higher than those of the thermally cycled large-die-attached samples, which were 1897 cycles and 1489 cycles, respectively. More thermal cycles means longer time spent at elevated temperature. The second possible explanation is based on the internal stress state difference between the small- and large-die-attached samples. It is known that the large-die-attached package has solder joint locations that experience higher stress during thermal cycling than the small-die-attached packages due to the CTE mismatch. If the internal stress is at a certain high level, the effect of microstructure and Sn grain orientation characteristics might not be so dominant, and thus the impact of transferred microstructure or evolution of the Sn grain structure does not significantly impact the overall characteristic lifetime cycle number degradation. If the internal stresses on certain solder joints are low, however, factors other than thermomechanical stress can exist and may play a larger role, which would accelerate the degradation of the characteristic lifetime cycle number after isothermal aging.

To further identify the reason for the difference in thermal cycling performance between the small- and large-die-attached samples, the crack location and distribution in the samples were first identified. A dye-and-pry process was applied, and Fig. 5 shows the resulting location summary map for small and large die sample sets. Six samples for each small- and large-die-attached sample were selected and subjected to dye and pry after thermal cycling. Locations indicated in red are the joint locations where most of the cracked joints are observed, and the blue areas are those that have the least number of cracks (blank box means no crack was found). As shown in Fig. 5a, for a small-die-attached sample, the most frequently cracked joint locations were at the inner edge of the package. All cracks were located at the package-side solder bulk region near the interface. The cracks were initiated at the upper corner of the package side and propagated through

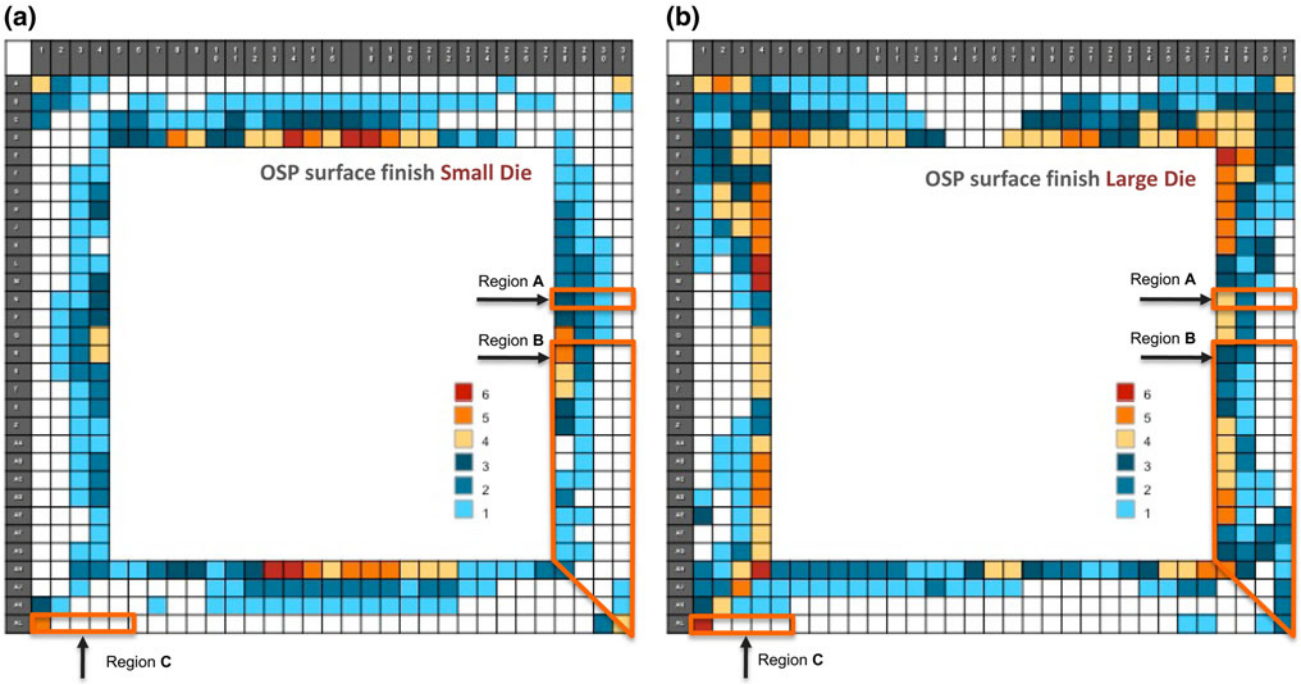

Fig. 5. Dye-and-pry result: fractured joint location summary map for (a) small-die-attached package samples and (b) large-die-attached package samples. Locations indicated as red are the joint locations where the most cracked joints were observed.

the upper part of the solder joint. The dye-and-pry results for the small- and large-die-attached samples are shown in Fig. 5b. Most of the failed joints are located at the corner of the package.

Finite-element method (FEM) simulation was employed to further understand how solder joint reliability interacts with the change in die size. Shown in Fig. 6 is a three-dimensional (3D) FEM model built with ANSYS.[18] Due to the symmetry, only 1/8 of the package has been included in the simulation, as shown in Fig. 6a. Package detail surrounding the solder joints has been constructed as seen in Fig. 6b; the detailed mesh of a joint is shown in Fig. 6c. All materials except solder joints were assumed to be linearly elastic. The thermo-mechanical properties used in the simulation are listed in the inset table of Fig. 6. A hyperbolic sine creep law was adopted for solder joints in the FEM model to capture the solder creep damage during thermal cycling:

$$\dot{\varepsilon}_{\mathrm{cr}} = C[\sinh(\alpha\sigma)]^{n}\exp\left[\frac{-Q}{\kappa T}\right],$$

where C, α, n, and Q are material constants.[19] The accumulated creep strain energy density was used to describe the cyclic damage buildup inside the solder material. The critical joint locations, based on the FEM modeling, matched well with the failure analysis findings. Figure 7a and b show the solder joint creep damage accumulation distributions for small- and large-die-attached samples from the area indicated as region B in Fig. 5, which represents the creep strain energy buildup in solder joints per cycle during accelerated thermal cycling due to the different die sizes.

As shown in Fig. 7, the stress state for each solder joint location is different and causes a different microstructural evolution history for each solder joint. The failure locations caused by thermal cycling, as revealed in the dye-and-pry results of Fig. 5, show the complexity of the stress states driven by thermal cycling and fatigue crack correlation. To analyze the microstructural evolution during thermal cycling for both small- and large-die-attached packages, the joints in region A and region C indicated in Fig. 5 were cross-sectioned and observed by optical microscopy with polarized filters and by OIM. The images in Fig. 8 are joint cross-section polarized images and OIM scan images of region C (indicated in Fig. 5). Figure 8a shows polarized images from a large-die-attached sample before thermal cycling. The joint indicated as joint C1 is the corner joint in the package. Most of the joints showed single-crystal joints and had no damage accumulation at either the package side or board side inside the bulk solder. Figure 8b shows OIM scanned images taken from the same joints as those shown in Fig. 8a. Each color represents the c-axis direction. A more detailed explanation can be found in other references.[14–17]

Figure 8c shows the cross-section of a large-die-attached sample at failure after thermal cycling. As shown in Fig. 8c, at joint C1, a crack developed and propagated through the joint, associated with a wide region of recrystallization near the crack

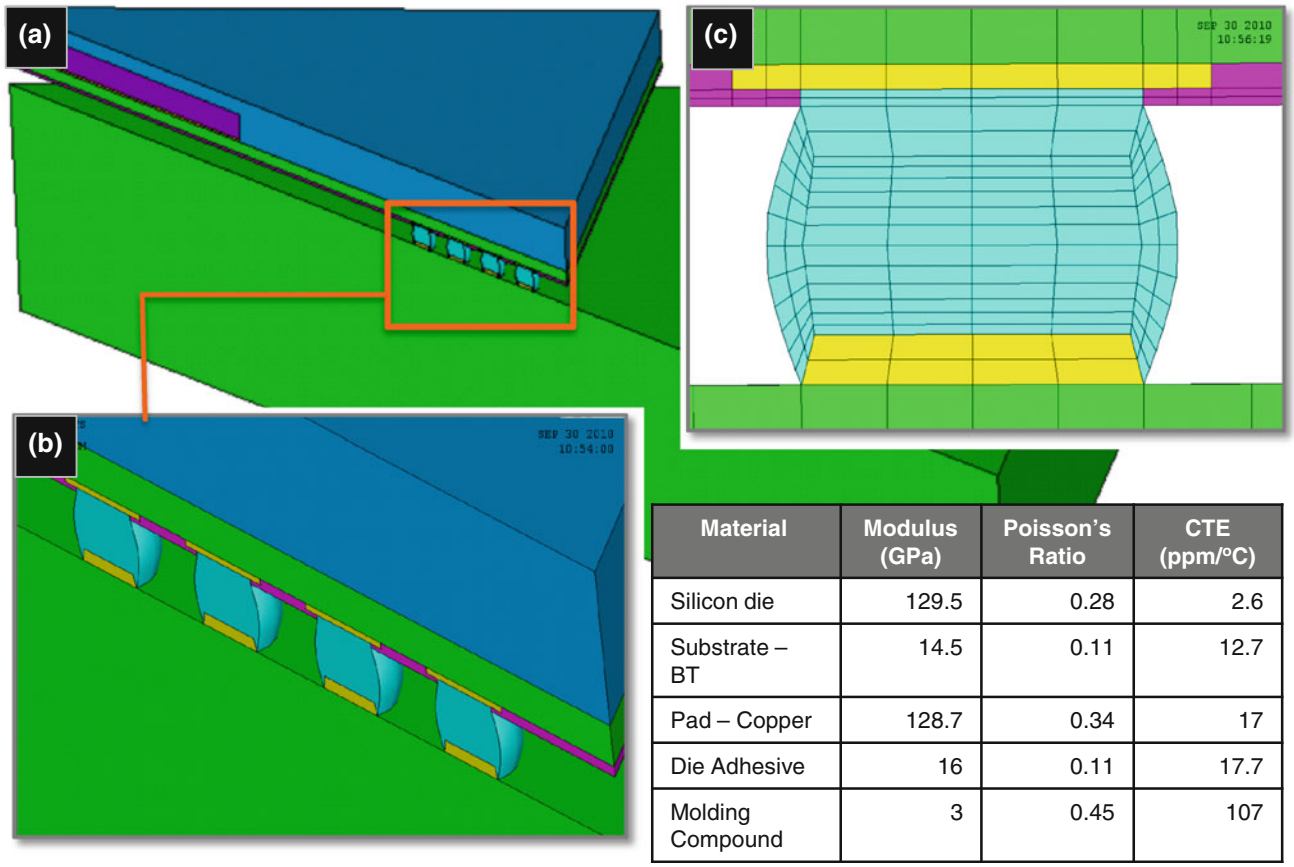

Material	Modulus (GPa)	Poisson's Ratio	CTE (ppm/°C)
Silicon die	129.5	0.28	2.6
Substrate – BT	14.5	0.11	12.7
Pad – Copper	128.7	0.34	17
Die Adhesive	16	0.11	17.7
Molding Compound	3	0.45	107

Fig. 6. One-eighth 3D FEM global model: (a) a small-die-package mounted on PCB, (b) local view of the FEM model to show structures surrounding solder joints, and (c) finite-element mesh on a solder joint.

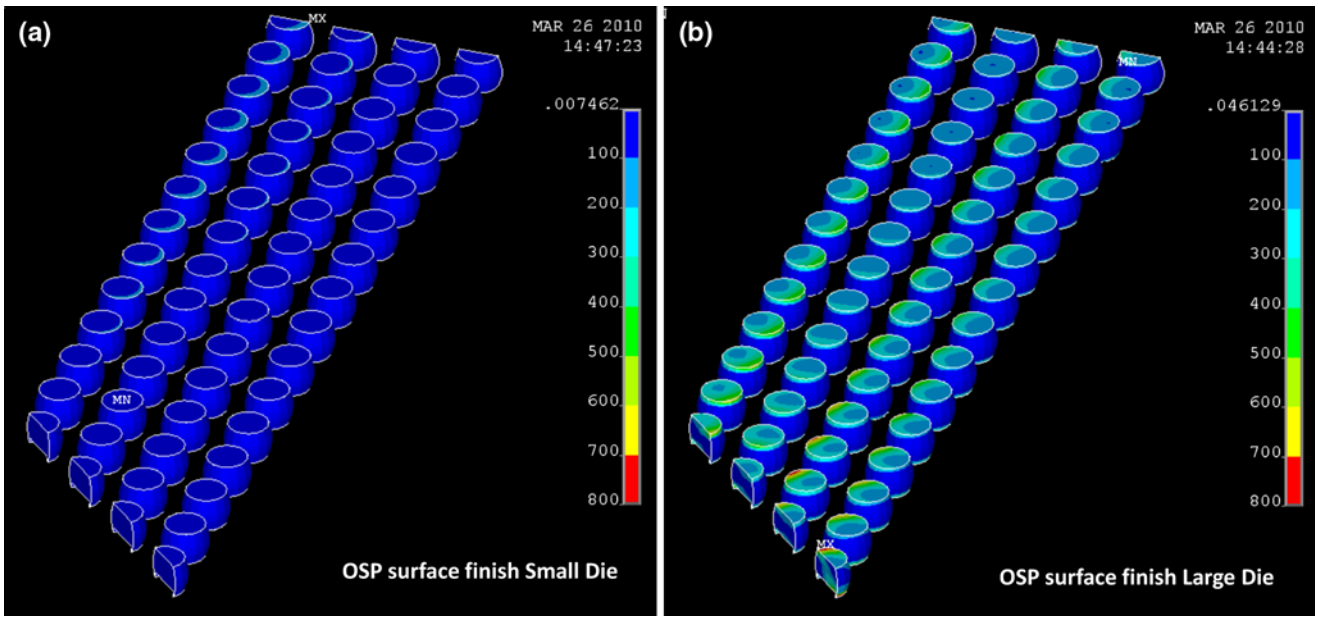

Fig. 7. FEM model of creep damage accumulation distribution from the region indicated as region B in Fig. 5: (a) small-die-attached package samples and (b) large-die-attached package samples.

propagation path, which can also be observed in joint C1 of Fig. 8d. Compared with the as-assembled and subsequently thermally cycled solder joints, the joints submitted to aging at 150°C for 500 h and then thermally cycled shown in Fig. 8e and f indicate more severe recrystallization. In addition, of

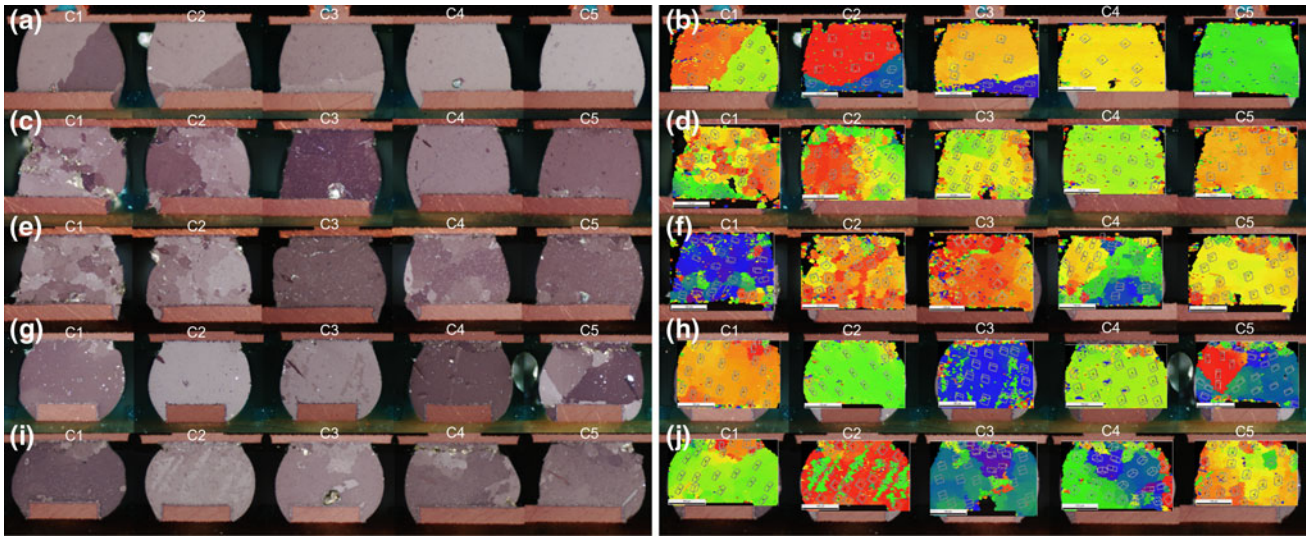

Fig. 8. Cross-section polarized images and OIM scanned images from the solder joints taken from the area indicated as region C in Fig. 5: (a) as-assembled and (b) OIM image associated with the cross-section in (a). (c) and (d) as-assembled and then thermally cycled large die attached sample. (e) and (f) 150°C/500 h aged and then thermally cycled large-die-attached sample. (g) and (h) as-assembled and then thermally cycled small-die-attached sample. (i) and (j) 150°C/500 h aged and then thermally cycled small-die-attached sample.

the as-assembled and thermally cycled joints, only C1 and C2 showed recrystallization and transformation into multicrystal joints. However, the joints submitted to aging and thermal cycling showed an overall transformation into multicrystals. From this, it was determined that thermally aged joints are easier to transform into multicrystal joints and, thus, more likely to show fatigue cracks. A more detailed explanation about the correlation between recrystallization and crack formation can be found in other publications.[20] This single-to-multicrystal trend is aligned with earlier findings published elsewhere.[15,17]

To compare with the large die packages, Fig. 8g–j shows cross-sections from small-die-attached samples. As shown in joint C1 of Fig. 8g and joint C1 of Fig. 8i, the damage accumulation in small die packages is less than that in large-die-attached samples. It was already shown in Fig. 7 that the corner joints are less stressed in the smaller die samples than those in the larger die samples, but compared with the as-assembled and subsequently thermally cycled sample, the isothermally aged and subsequently thermally cycled sample showed a higher rate of multicrystal transformation. Based on this series of observations, it is confirmed that the higher stress during thermal cycling causes higher multicrystal orientation, and with isothermally aged solder joints, it seems that, for a given stress state, the deformation is more severe and shows more damage accumulation. This can be explained by the higher creep rate after aging.[5,12] The higher creep rate in aged solder joints can allow more strain or plastic deformation for a given stress, and the damage accumulation can be transformed into recrystallization or grain rotation during thermal cycling, where the temperature varies from 0°C to 100°C.

The same phenomena can be observed in Fig. 9. Figure 9 shows cross-sectional images from region A indicated in Fig. 5. Unlike the corner joints shown in Fig. 8, these joints are from the inner edge toward the outer edge of the package. Figure 9a, b shows the joints before thermal cycling, and Fig. 9c, d shows the joints after thermal cycling with no preaging condition and with a large die attached. The die edge is located above joint A3, and joint A1 is the joint at the inner edge; joint A4 is the joint at the outer edge of the package. The solder cross-section shows localized recrystallization at joint A4, but most of the other cross-sections are not affected and show less single-to-multicrystal transformation. Compared with the as-assembled and thermally cycled joints, the cross-sections after aging shown in Fig. 9e, f show an overall single-to-multicrystal transformation and, thus, produced more cracks in the solder joint. The same trend can be observed in Fig. 9g–j, which shows cross-sections of samples with a small die attached. Localized recrystallization is observed in Fig. 9h joint A1; the other joints in the same row did not show much damage compared with the aged and thermally cycled joints in Fig. 9i, j.

Along with Sn grain recrystallization and the internal stress distribution effect, a precipitate depletion zone is also observed in small-die-attached samples. As shown in Fig. 10, fatigue cracks are initiated and propagate near the package-side interface inside the solder bulk area. High-magnification SEM images are shown in Fig. 11. Figure 11a–c shows the crack development in samples with a small die attached. Compared with the as-assembled joint in Fig. 11a associated with the IMC growth at the interface, a clear depletion zone without IMC precipitates is observed near the

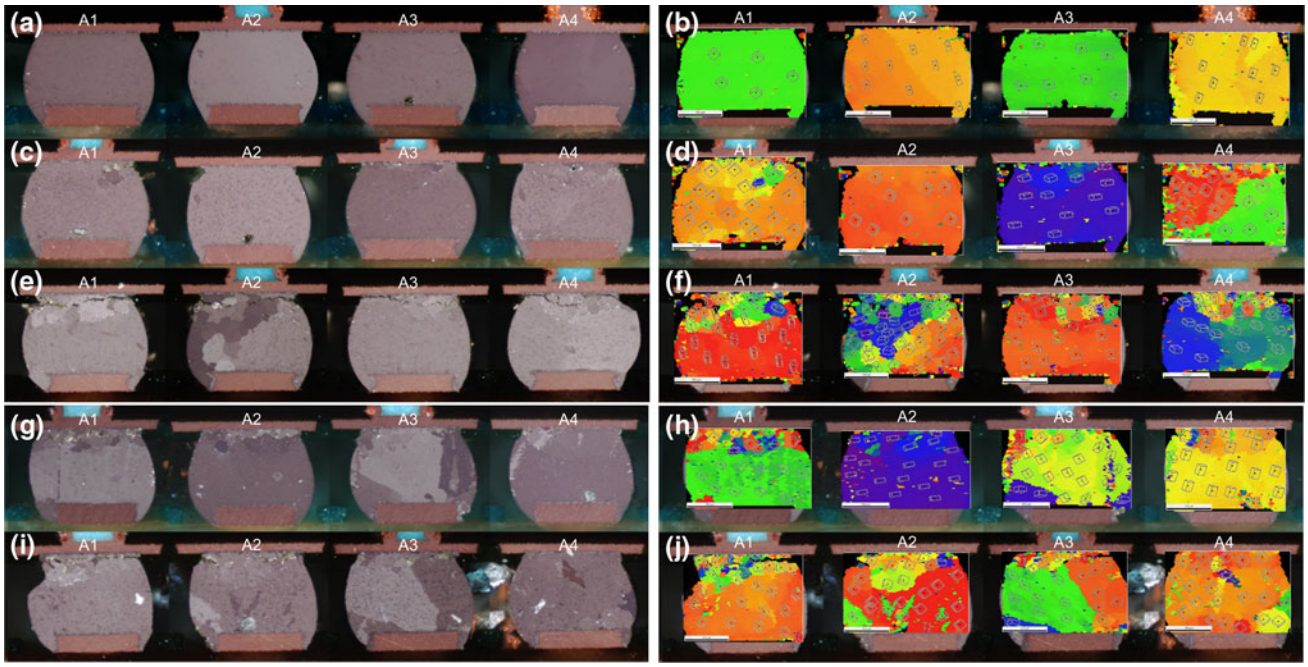

Fig. 9. Cross-section polarized images and OIM scanned images from solder joints taken from the area indicated as region A in Fig. 5: (a) as-assembled and (b) OIM image associated with the cross-section in (a). (c) and (d) as-assembled and then thermally cycled large-die-attached sample. (e) and (f) 150°C/500 h aged and then thermally cycled large-die-attached sample. (g) and (h) as-assembled and then thermally cycled small-die-attached sample. (i) and (j) 150°C/500 h aged and then thermally cycled small-die-attached sample.

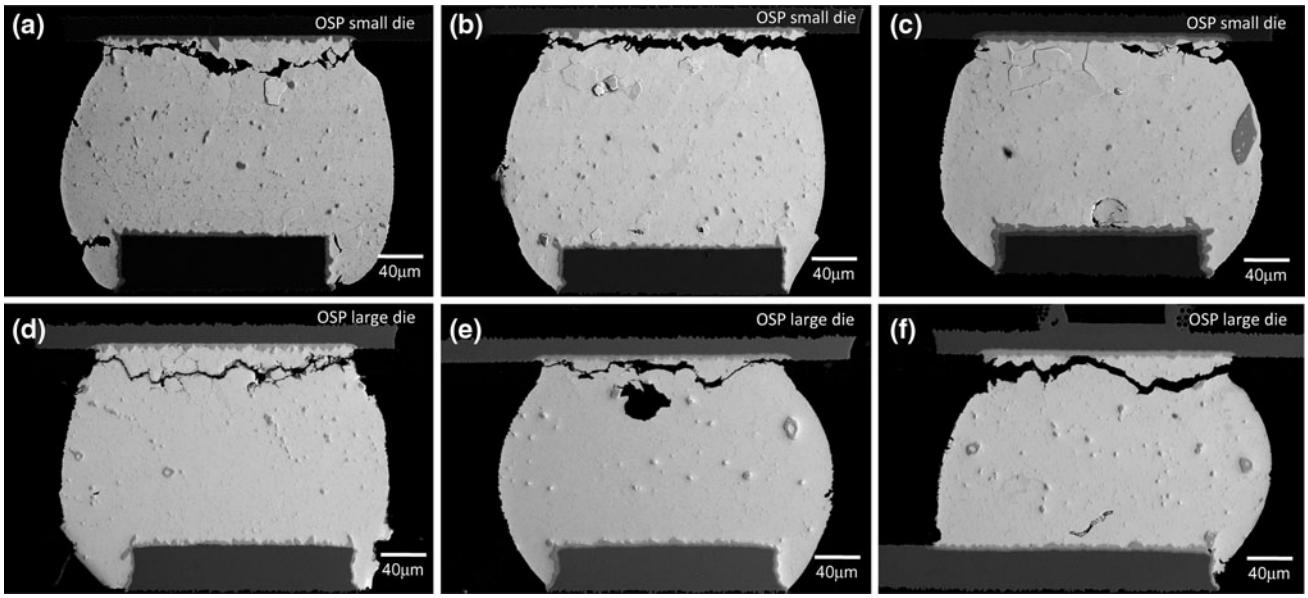

Fig. 10. SEM microstructure after isothermal aging and thermal cycling: (a) unaged as-assembled small-die-attached samples after thermal cycling, (b) after aging at 100°C/1000 h aging + thermal cycling, and (c) after 150°C/1000 h aging + thermal cycling. (d) Unaged, as-assembled large-die-attached samples after thermal cycling, (e) aging at 150°C/500 h aging + thermal cycling, and (f) after 150°C/1000 h aging + thermal cycling.

interface in samples isothermally aged at 150°C for 1000 h and subsequently thermally cycled (Fig. 11-c). This trend is not observed in the large-die-attached samples shown in Fig. 11d–f. As explained in an earlier publication,[13] the pre-existing IMC precipitates near the interface show a tendency to coalesce but maintain their locations and still reside near the interface and the propagated cracks even after isothermal aging and thermal cycling. These series of observations provides a possible explanation regarding the higher rate of characteristic lifetime reduction after isothermal aging with

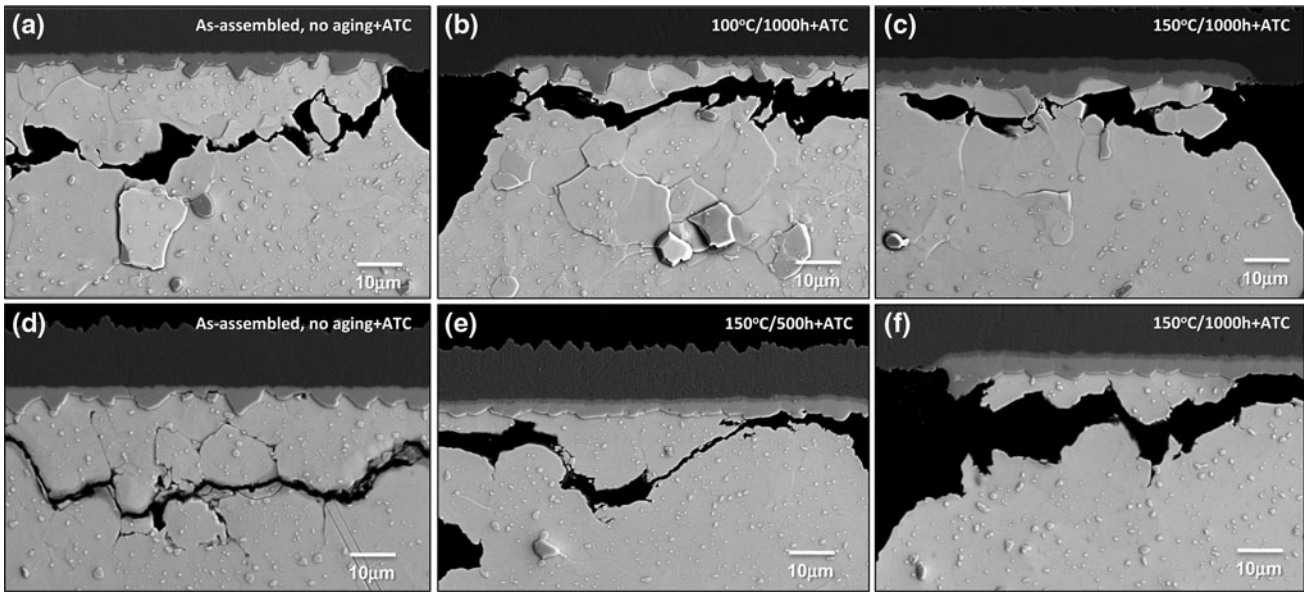

Fig. 11. SEM microstructure after isothermal aging and thermal cycling (higher-magnification images from Fig. 10): (a) unaged as-assembled small-die-attached samples after thermal cycling, (b) after aging at 100°C/1000 h aging + thermal cycling, and (c) after 150°C/1000 h aging + thermal cycling. (d) Unaged as-assembled large-die-attached samples after thermal cycling, (e) aging at 150°C/500 h aging + thermal cycling, and (f) after 150°C/1000 h aging + thermal cycling.

small-die-attached OSP-surface-finished samples compared with their larger counterparts. Both small- and large-die-attached samples show a higher rate of transformation from single- to multicrystals during thermal cycling after isothermal aging. However, if the internal stress is already at a certain high level, the effects of microstructure and Sn grain orientation contribute less and do not significantly impact the overall degradation of the characteristic lifetime cycle number, resulting in less degradation of the characteristic lifetime after isothermal aging. However, if the internal stresses in certain solder joints are low, factors other than pure thermomechanical stress can exist and play a large role, which would accelerate the degradation of the characteristic lifetime after isothermal aging. In this case, the combination of longer thermal cycling time, higher rate of single-to-multicrystal transformation after aging, and higher rate of crack initiation in multicrystallized solder joints augment the effect of isothermal aging and contribute to a higher rate of characteristic lifetime degradation during thermal cycling.

CONCLUSIONS

The interaction between isothermal aging and long-term reliability of fine-pitch BGA packages with two different die sizes was investigated. Both small- and large-die-attached packages with Sn-3.0Ag-0.5Cu (wt.%) solder balls were used to compare the correlation between the internal strain difference and isothermal aging on microstructure evolution during thermal cycling. The packages with large dies attached showed shorter lifetimes because of the relatively higher stress present in them but were less affected by isothermal aging than the small-die-attached samples. Microstructural analysis using OIM revealed the evolution of the microstructure during thermal cycling, which showed a higher degree of recrystallization inside the bulk solder for higher-stress joints and joints that were isothermally aged. If the internal stress is already at a certain high level, the effects of microstructure and Sn grain orientation contribute less and do not significantly impact the overall characteristic lifetime cycle number degradation, resulting in less degradation of the characteristic lifetime after isothermal aging. However, if the internal stresses in certain solder joints are low, factors other than pure thermomechanical stress can exist and play a large role, which would accelerate the degradation of the characteristic lifetime cycle number after isothermal aging. In this study, it is determined that the combination of longer thermal cycling time, higher rate of single-to-multicrystal transformation after aging, and higher rate of crack initiation in multicrystallized solder joints augments the effect of isothermal aging and contributes to a higher rate of characteristic lifetime degradation during thermal cycling.

ACKNOWLEDGEMENTS

This work is a research project supported by the Cisco Component Quality and Technology group in the Technology and Quality group.

REFERENCES

1. J. Glazer, *Int. Mater. Rev.* 40, 65 (1995).
2. H.K. Kim and K.N. Tu, *Phys. Rev. B* 53, 16027 (1996).
3. J. Glazer, *J. Electron. Mater.* 23, 8 (1994).
4. W. Xie, T.-K. Lee, K.-C. Liu, and J. Xue, IEEE 60th Electronic Components and Technology Conference (ECTC), Las Vegas, NV, June (2010).
5. H.G. Song, J.W. Morris Jr., and F. Hua, *JOM* 56, 30 (2002).
6. K.W. Moon, W.J. Boettinger, U.R. Kattner, F.S. Biancaniello, and C.A. Handwerker, *J. Electron. Mater.* 29, 1122 (2000).
7. D.R. Frear and P.T. Vianco, *Metall. Trans. A* 25A, 1509 (1994).
8. W.K. Choi and H.M. Lee, *J. Electron. Mater.* 29, 10 (2000).
9. A.J. Sunwoo, J.W. Morris Jr., and G.K. Lucey Jr., *Metall. Trans. A* 23A, 1323 (1992).
10. Z. Mei and J.W. Morris, *J. Electron. Mater.* 21, 599 (1992).
11. F. Bartels, J.W. Morris Jr., G. Dalke, and W. Gust, *J. Electron. Mater.* 23, 787 (1994).
12. H. Ma, J.C. Suhling, P. Lall, and M.J. Bozack, Proceeding of the 56th Electronic Components and Technology Conference, San Diego, California, May (2006).
13. T.-K. Lee, M. Hongtao, and K.-C. Liu, *J. Electron. Mater.* 39, 2564 (2010).
14. T.R. Bieler, T.-K. Lee, and K.-C. Liu, *J. Electron. Mater.* 38, 2712 (2009).
15. T.-K. Lee, K.-C. Liu, and T.R. Bieler, *J. Electron. Mater.* 38, 2685 (2009).
16. B. Zhou, T.R. Bieler, T.-K. Lee, and K.-C. Liu, *J. Electron. Mater.* 38, 2702 (2009).
17. T.-K. Lee, B. Zhou, T.R. Bieler, and K.-C. Liu, *J. Electron. Mater.* 39, 2588 (2010).
18. ANSYS Inc., ANSYS Mechanical V12, (2010).
19. A. Schubert, R. Dudek, E. Auerswald, A. Gollhart, B. Michael, and H. Reichl, IEEE 53th Electronic Components and Technology Conference (ECTC), New Orleans, LA, June (2003).
20. B. Zhou, T.R. Bieler, T.-K. Lee, and K.-C. Liu, *J. Electron. Mater.* 39, 2669 (2010).